Available online at www.sciencedirect.com
SCIENCE DIRECT
Journal of Sound and Vibration 295 (2006) 614–632
JOURNAL OF SOUND AND VIBRATION
www.elsevier.com/locate/jsvi

Determining the strength of rotating broadband sources in ducts by inverse methods

C.R. Lowis*, P.F. Joseph

Institute of Sound and Vibration Research, University of Southampton, Highfield, Southampton SO17 1BJ, UK

Received 24 June 2005; received in revised form 21 December 2005; accepted 10 January 2006
Available online 20 March 2006

Abstract

Aeroengine broadband fan noise is a major contributor to the community noise exposure from aircraft. It is currently believed that the dominant broadband noise mechanisms are due to interaction of the turbulent wake from the rotor with the stator, and interaction of the turbulent boundary layers on the rotor blades with their trailing edges. Currently there are no measurement techniques that allow the localisation and quantification of rotor-based broadband noise sources. This paper presents an inversion technique for estimating the broadband acoustic source strength distribution over a ducted rotor using pressure measurements made at the duct wall. It is shown that the rotation of acoustic sources in a duct prevents the use of standard acoustic inversion techniques. A new technique is presented here for inverting the strength of rotating broadband sources that makes use of a new Green function taking into account the effect of source rotation. The new Green function is used together with a modal decomposition technique to remove the effect of source rotation, thereby allowing an estimation of the rotor-based source strengths in the rotating reference frame. It is shown that the pressure measured at the sensors after application of this technique is identical to that measured by sensors rotating at the same speed as the rotor. Results from numerical simulations are presented to investigate the resolution limits of the inversion technique. The azimuthal resolution limit, namely the ability of the measurement technique to discriminate between sources on adjacent blades, is shown to improve as the speed of rotation increases. To improve the robustness of the inversion technique, a simplifying assumption is made whereby the sources on different blades are assumed to be identical. It is also shown that the accuracy and robustness of the inversion procedure improve as the axial separation between the rotor and sensors decreases. Simulation results demonstrate that for a 26-bladed fan, rotating with a blade tip Mach number of $M_t = 0.5$, the aerodynamic source strengths can be estimated with acceptable robustness and approximately 1 dB accuracy, when measurements are made approximately 0.1 acoustic wavelengths from the rotor.

1. Introduction

Broadband aeroengine fan noise is becoming increasingly important to the overall noise from aeroengines as the effectiveness of methods for reducing tonal noise steadily improve. This paper describes an experimental method for determining the broadband acoustic source strength distribution over the surface of a ducted rotor

*Corresponding author. Tel.: +44 23 80 592196; fax: +44 23 80 593190.
E-mail addresses: cl@isvr.soton.ac.uk (C.R. Lowis), pfj@isvr.soton.ac.uk (P.F. Joseph).

0022-460X/$ - see front matter © 2006 Elsevier Ltd. All rights reserved.
doi:10.1016/j.jsv.2006.01.031

using pressure measurements made at the duct wall. The motivation for this work is the current lack of measurement techniques that allow the quantification of the broadband source strengths over a ducted rotor.

A method to locate the effective acoustic sources on an *open* rotor was presented by Sijtsma et al. [1]. The technique uses a far-field microphone array, and a conventional time domain delay and sum beamforming algorithm to steer the beam over the rotor blades, whilst rotating it at the angular frequency of the rotor. The technique was applied to a 4.5 m diameter, two-bladed wind turbine. The dominant broadband aerodynamic sources were clearly identified as originating at the trailing edges of the individual rotor blades.

Another class of methods that have been used for source strength localisation and quantification are known as inversion techniques. Acoustic source strengths are deduced from measurements of acoustic pressure by inverting a transfer matrix of source–receiver Green functions. Inversion techniques have been used in free-field applications [2–4] where the radiation paths can be modelled by simple analytical Green functions.

The first attempt to apply inversion techniques to non–rotating sources in a duct was proposed by Kim and Nelson [5]. An analytic hard-walled, finite length, no-flow duct Green function was used to determine the source strength and location of a single stationary loudspeaker in a duct of 0.315 m radius with one open, and one anechoically terminated end. The radial and axial locations of the source was assumed to be known, and the technique was used to determine the azimuthal position, and the strength of the source. At a normalised frequency of $ka = 1.57$ the azimuthal location of the source could be determined to within 30° and its strength to within 3 dB when acoustic pressure measurements were made 0.05 m (approx 0.04λ) from the source plane.

Numerical simulations were performed to investigate the effect of different source and receiver geometries on the conditioning of the inverse problem. For a fixed measurement position the transfer matrix was shown to become ill-conditioned as the distance between assumed sources decreased. It was shown that, to achieve higher spatial resolution, measurements have to be made in the near field of the sources. This finding is consistent with the source strength measurement requirements of acoustic near field holography [6].

While the work of Kim and Nelson used a Green function obtained from a numerical model, Holland [7] has shown that, in a reverberant environment, measured Green functions can also be used. This suggests that the application of inversion techniques to ducted sources is not limited by a requirement for an accurate theoretical model of the sound propagation, provided a source–receiver Green function, or its reciprocal, can be measured.

This paper extends the work of Sijtsma et al. and Kim and Nelson to the inversion of *rotating*, *broadband*, aerodynamic sources on a ducted rotor. The equivalent uncorrelated sources in this case are shown to be separated by a correlation length that will be shown to be typically an order of a magnitude smaller than an acoustic wavelength. The resolution of sources at this separation distance necessitates the use of pressure measurements made in the near field of the rotor. The technique proposed here, unlike the technique proposed by Sijtsma et al., is based in the frequency domain. The novel aspect of this measurement procedure is that it provides a means to remove the effect of source rotation and hence allows the inversion of ducted broadband sources in the rotating reference frame.

2. Theory

2.1. Sound field due to a rotating dipole source distribution in an infinite duct with flow

Consider an infinite hard-walled cylindrical duct containing a uniform axial mean flow as shown in Fig. 1. The broadband acoustic source strength distribution due to a rotating fan blade is represented by acoustic dipole sources distributed over the blade surfaces with specified spatial and frequency correlation characteristics. The sources, with dipole moment distribution specified by $\mathbf{f}(\mathbf{y},\tau) = \mathbf{f}(r_s, \theta_s - \Omega\tau, z_s, \tau)$, are assumed to rotate around the duct axis in the θ-direction at an angular frequency Ω.

In the absence of stator vanes, the dominant broadband noise sources are situated on the rotor, and arise due to the interaction of the turbulent boundary produced on the surface of the rotor blades with the fan blade trailing edges.

Putting $\mathbf{f}(\mathbf{y},\tau) = f(\mathbf{y},\tau)\hat{\mathbf{n}}(\mathbf{y})$, where $\hat{\mathbf{n}}(\mathbf{y})$ is the unit vector normal to the blade surface, S, the time-varying pressure at any receiver point $\mathbf{x} = (r,\theta,z)$ within the duct can be calculated from the Green function solution

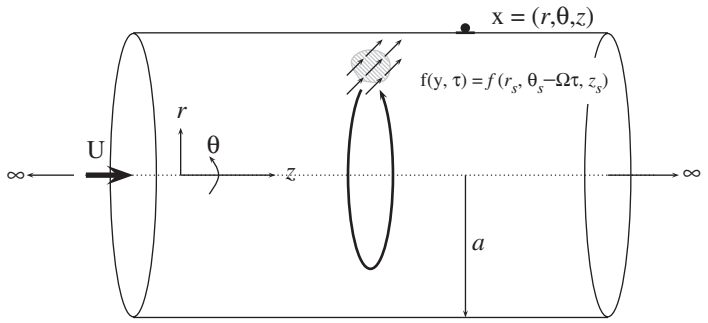

Fig. 1. A dipole source distribution rotating at angular speed Ω radiates sound in an infinite hard-walled cylindrical duct with superimposed mean flow.

to the wave equation,

$$p(\mathbf{x},t)=\int_{-T}^{+T}\int_{S} f(\mathbf{y},\tau)\hat{\mathbf{n}}(\mathbf{y})\cdot\nabla G(\mathbf{x},t|\mathbf{y},\tau)\,\mathrm{d}S(\mathbf{y})\,\mathrm{d}\tau, \tag{1}$$

where $f(\mathbf{y},\tau)$ is the magnitude of the dipole source strength distribution over the surface of the rotor blades. Note that source position is a function of emission time τ, $\mathbf{y}=\mathbf{y}(\tau)$.

The Green function solution for an infinite, hard-walled cylindrical duct containing an axial uniform mean flow with velocity U may be expressed as a superposition of an infinite number of modes given by, amongst others, Goldstein [8],

$$G(\mathbf{x},t|\mathbf{y},\tau)=\frac{\mathrm{i}}{4\pi}\sum_{m=-\infty}^{\infty}\sum_{n=0}^{\infty}\frac{\psi_{mn}(r)\psi^{*}_{mn}(r_s)\mathrm{e}^{\mathrm{i}m(\theta-\theta_s)}}{\Lambda_{mn}}\int_{-\infty}^{\infty}\frac{\mathrm{e}^{\mathrm{i}\omega(t-\tau)}\mathrm{e}^{-\mathrm{i}\gamma^{\pm}_{mn}(z-z_s)}}{\kappa_{mn}(\omega)}\,\mathrm{d}\omega, \tag{2}$$

where ψ_{mn} denotes the radial mode shape function of the $(m,n)^{\text{th}}$ mode, which in a hollow duct is of the form,

$$\Psi_{mn}(r)=J_m\left(\sigma_{mn}\frac{r}{a}\right) \tag{3}$$

where J_m is the first-order Bessel function of order m. In a hard-walled cylindrical duct, σ_{mn} is the n^{th} stationary value of the Bessel function of order m. The term Λ_{mn} is introduced to ensure the mode normalisation condition,

$$2\pi\Lambda_{mn}^{-1}\int_0^a|\psi_{mn}(r)|^2 r\,\mathrm{d}r=1, \tag{4}$$

where a is the duct radius.

Substituting the Green function of Eq. (2) into the convective wave equation leads to the following expressions for the mode wavenumbers κ and γ [9],

$$\gamma^{\pm}_{mn}=\frac{-Mk\mp\kappa_{mn}}{1-M^2},\quad \kappa_{mn}=\sqrt{k^2-(1-M^2)\left(\frac{\sigma_{mn}}{a}\right)^2}, \tag{5}$$

where $M=U/c$ is the axial flow Mach number.

Modes can propagate unattenuated when κ_{mn} is real. From Eq. (5) this leads to an expression for the cut-on frequency associated with each mode. In normalised duct-frequency units, it is given by

$$(ka)_{mn}=\sigma_{mn}\sqrt{1-M^2}. \tag{6}$$

At a frequency below the cuton frequency the modes decay exponentially along the duct.

A dipole source aligned at an angle β relative to the duct axis has components of $\hat{\mathbf{n}}$ given by

$$\hat{\mathbf{n}}=[\hat{r},\hat{\theta},\hat{z}]=[0,\sin\beta,\cos\beta], \tag{7}$$

where in general $\beta = \beta(\mathbf{y})$. The ∇ operator in cylindrical coordinates is given by

$$\nabla G = \hat{r}_s \frac{\partial G}{\partial r_s} + \frac{\hat{\theta}}{r_s}\frac{\partial G}{\partial \theta_s} + \hat{\mathbf{z}}\frac{\partial G}{\partial z_s}. \tag{8}$$

Substituting Eq. (2) into Eq. (8) gives the non-zero components of ∇G as

$$\frac{\hat{\theta}}{r_s}\frac{\partial G}{\partial \theta_s} = \frac{\mathrm{i}\hat{\theta}}{4\pi}\sum_{m=-m_0}^{m_0}\frac{-\mathrm{i}m}{r_s}\sum_{n=0}^{n_0}\frac{\psi_{mn}(r)\psi^*_{mn}(r_s)\mathrm{e}^{\mathrm{i}m(\theta-\theta_s)}}{\Lambda_{mn}}\int_{-\infty}^{\infty}\frac{\mathrm{e}^{\mathrm{i}\omega(t-\tau)}\mathrm{e}^{-\mathrm{i}\gamma^{\pm}_{mn}(z-z_s)}}{\kappa_{mn}(\omega)}\,\mathrm{d}\omega, \tag{9}$$

$$\hat{\mathbf{z}}\frac{\partial G}{\partial z_s} = \frac{\mathrm{i}\hat{\mathbf{z}}}{4\pi}\sum_{m=-m_0}^{m_0}\sum_{n=0}^{n_0}\mathrm{i}\gamma^{\pm}_{mn}\frac{\psi_{mn}(r)\psi^*_{mn}(r_s)\mathrm{e}^{\mathrm{i}m(\theta-\theta_s)}}{\Lambda_{mn}}\int_{-\infty}^{\infty}\frac{\mathrm{e}^{\mathrm{i}\omega(t-\tau)}\mathrm{e}^{-\mathrm{i}\gamma^{\pm}_{mn}(z-z_s)}}{\kappa_{mn}(\omega)}\,\mathrm{d}\omega. \tag{10}$$

For receivers located several wavelengths from the sources, cutoff modes can be neglected and the modal summation is confined to the propagating modes, such that m_0 is the highest propagating azimuthal mode order, and n_0 the highest propagating radial mode order. Substituting Eqs. (9) and (10) into Eq. (1) gives

$$p(\mathbf{x},t) = \frac{1}{2\pi}\int_{-T}^{T}\int_{S} f(\mathbf{y},\tau)\sum_{m=-m_0}^{m_0}\int_{-\infty}^{\infty} g_m(\mathbf{y},z,r,\omega)\mathrm{e}^{\mathrm{i}m\theta}\mathrm{e}^{\mathrm{i}\omega(t-\tau)}\,\mathrm{d}\omega\,\mathrm{d}S(\mathbf{y})\,\mathrm{d}\tau, \tag{11}$$

where for conciseness a transfer impedance, g_m, has been defined which relates the pressure due to a spinning mode of order m at a frequency ω, located at $\mathbf{x} = (r, \theta = 0^\circ, z)$, due to a point dipole source of unit source strength located at $\mathbf{y}$. It is obtained by comparing Eq. (11) with the result of substituting Eqs. (9) and (10) into Eq. (1),

$$g_m(\mathbf{y},z,r,\omega) = \frac{1}{2}\sum_{n=0}^{n_0}\left[-\gamma^{\pm}_{mn}\cos\beta + \frac{m}{r_s}\sin\beta\right]\frac{\psi_{mn}(r)\psi^*_{mn}(r_s)\mathrm{e}^{-\mathrm{i}m\theta_s}}{\Lambda_{mn}}\,\frac{\mathrm{e}^{-\mathrm{i}\gamma^{\pm}_{mn}(z-z_s)}}{\kappa_{mn}(\omega)}. \tag{12}$$

2.2. Sound field produced by a broadband rotating dipole source distribution

For rotating sources the circumferential source position $\theta_s(\tau)$ in the stationary reference frame (relative to the duct) may be related to the angle $\tilde{\theta}_s$ in a rotating reference frame spinning with the rotor at an angular frequency Ω by $\theta_s = \tilde{\theta}_s - \Omega\tau$; where Ω is the shaft rotation frequency. Substituting for θ_s in Eq. (11), the expression for p becomes

$$p(\mathbf{x},t) = \frac{1}{2\pi}\int_{-T}^{T}\int_{\tilde{S}} f(\tilde{\mathbf{y}},\tau)\sum_{m=-m_0}^{m_0}\int_{-\infty}^{\infty} g_m(\tilde{\mathbf{y}},z,r,\omega)\mathrm{e}^{\mathrm{i}m\theta}\mathrm{e}^{\mathrm{i}\omega t-\mathrm{i}(\omega-m\Omega)\tau}\,\mathrm{d}\omega\,\mathrm{d}\tilde{S}(\tilde{\mathbf{y}})\,\mathrm{d}\tau, \tag{13}$$

where $\tilde{\mathbf{y}}$ is the time-independent source position evaluated in the rotating reference frame, $\tilde{\mathbf{y}} = (r_s, \tilde{\theta}_s, z_s)$ and $\tilde{S} = \tilde{S}(\tilde{\mathbf{y}})$.

The integral over τ in Eq. (13) is of the form

$$\int_{-T}^{T} f(\tilde{\mathbf{y}},\tau)\mathrm{e}^{-\mathrm{i}(\omega-m\Omega)\tau}\,\mathrm{d}\tau = f(\tilde{\mathbf{y}},\omega-m\Omega) \tag{14}$$

and Eq. (13) can therefore be written as

$$p(\mathbf{x},t) = \frac{1}{2\pi}\int_{\tilde{S}}\sum_{m=-m_0}^{m_0} f(\tilde{\mathbf{y}},\omega-m\Omega)\int_{-\infty}^{\infty} g_m(\tilde{\mathbf{y}},z,r,\omega)\mathrm{e}^{\mathrm{i}m\theta}\mathrm{e}^{\mathrm{i}\omega t}\,\mathrm{d}\omega\,\mathrm{d}\tilde{S}(\tilde{\mathbf{y}}). \tag{15}$$

Comparison of Eq. (15) with the definition of the Fourier transform,

$$p(\mathbf{x},t) = \frac{1}{2\pi}\int_{-\infty}^{\infty} p(\mathbf{x},\omega)\mathrm{e}^{\mathrm{i}\omega t}\,\mathrm{d}\omega \tag{16}$$

allows Eq. (15) to be written in the frequency domain as

$$p(\mathbf{x},\omega)=\int_{\tilde{S}}\sum_{m=-m_0}^{m_0} f(\tilde{\mathbf{y}},\omega-m\Omega)g_m(\tilde{\mathbf{y}},z,r,\omega)\mathrm{e}^{\mathrm{i}m\theta}\,\mathrm{d}\tilde{S}(\tilde{\mathbf{y}}). \tag{17}$$

Note that the effect of transforming the source integral to the rotating reference frame has been to shift the source frequency ω by $-m\Omega$. This finding will form the basis of the inversion procedure presented in Section 3.

Broadband sound fields are most suitably expressed in terms of the cross-spectrum between two points $\mathbf{x}$ and $\mathbf{x}'$ in the duct, defined by

$$S_{pp}(\mathbf{x},\mathbf{x}',\omega)=\lim_{T\to\infty}\frac{\pi}{T}E\{p(\mathbf{x},\omega)p^*(\mathbf{x}',\omega)\}, \tag{18}$$

where E denotes the expectation value.

Substituting Eq. (17) into Eq. (18) gives the following expression for S_{pp}

$$\begin{aligned}S_{pp}(\mathbf{x},\mathbf{x}',\omega)=&\int_{\tilde{S}}\int_{\tilde{S}'}\sum_{m=-m_0}^{m_0}\sum_{m'=-m_0}^{m_0} S_{ff}(\tilde{\mathbf{y}},\tilde{\mathbf{y}}',\omega-m\Omega,\omega-m'\Omega)\\&\times g_m(\tilde{\mathbf{y}},z,r,\omega)g^*_{m'}(\tilde{\mathbf{y}}',z,r',\omega)\mathrm{e}^{\mathrm{i}m\theta-\mathrm{i}m'\theta'}\,\mathrm{d}\tilde{S}(\tilde{\mathbf{y}})\,\mathrm{d}\tilde{S}(\tilde{\mathbf{y}}'),\end{aligned} \tag{19}$$

where

$$S_{ff}(\tilde{\mathbf{y}},\tilde{\mathbf{y}}',\omega,\omega')=\frac{\pi}{T}E\{f(\tilde{\mathbf{y}},\omega)f^*(\tilde{\mathbf{y}}',\omega')\}. \tag{20}$$

Eq. (19) is an expression for the pressure cross-spectrum between any two points in the duct due to a rotating dipole source distribution with spatial and frequency cross-spectra spectrum S_{ff} (in the rotating reference frame). Note that for rotating sources, $\Omega\neq 0$, the source strength and its propagation become coupled through the spinning mode index m. This is the reason why conventional inversion procedures, valid for stationary sources, for example as described by Kim and Nelson [5], cannot be applied to rotating sources. An alternative procedure is proposed in Section 3.

3. Inversion technique for ducted rotating sources

This section is concerned with an inversion technique to determine the broadband strengths of rotating broadband sources in a duct from a number of measurements of acoustic pressure made at the duct wall. We show below that their determination by existing inverse methods cannot be performed. A new technique for the inversion of rotating broadband sources is therefore proposed. Simulation results are presented to illustrate the various properties of the new inversion technique. Before presentation of the technique for inverting rotating sources, we first review the theory for the inversion of stationary source strengths. We will show subsequently that by appropriately processing the measured pressure signals, and by the introduction of a new Green function, the theory for the inversion of rotating sources may be written in an identical form to that for stationary sources.

3.1. Inversion techniques for stationary sources

Inverse techniques require the approximation of a continuous source region by a finite number of discrete sources (Fig. 2). The objective of the inversion procedure is to deduce the vector of optimal discretised source strengths, $\hat{\mathbf{f}}$, which in a model of the radiated sound field, $\mathbf{p}=\mathbf{G}\mathbf{f}$, matches, in a least-squares sense, the pressure $\hat{\mathbf{p}}$ measured at an array of microphones, where $\mathbf{G}$ is a matrix of transfer impedances, which may be measured or predicted.

At a single frequency the vector of pressures $\mathbf{p}$ due to a discretised *stationary* source distribution $\mathbf{f}$ can be written in the form

$$\mathbf{p}=\mathbf{G}\mathbf{f}, \tag{21}$$

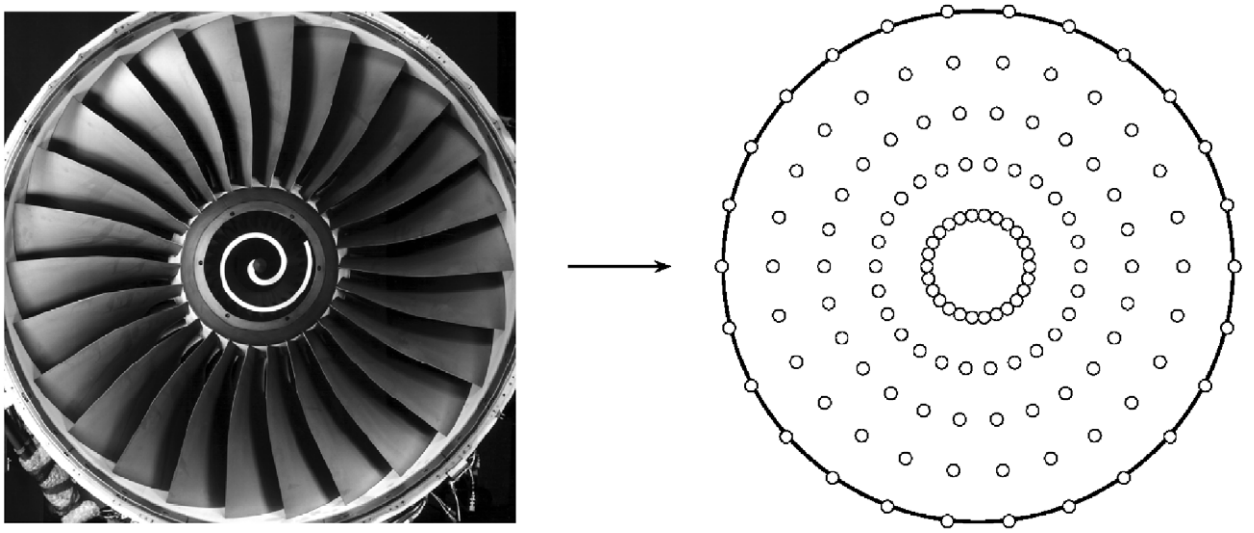

Fig. 2. An acoustic inversion problem is formulated by replacing the real acoustic source (left) with an equivalent distribution of discrete model sources (right).

where $\mathbf{G}$ is a matrix of transfer impedances that relates the assumed source distribution $\mathbf{f}$ to the vector of predicted pressures at the sensors. The $(i,j)^{\text{th}}$ element of $\mathbf{G}$ specifies the transfer impedance between the i^{th} source and the pressure at the J^{th} sensor. Note that, as indicated in Eq. (15), when there is relative motion between the source and receiver, the source and receiver frequencies are no longer identical.

In practice, the measured pressure signals are contaminated by "noise". Noise could be introduced by errors in the measurements and also by inaccuracies in the model of $\mathbf{G}$. We therefore write the vector of measured pressures $\hat{\mathbf{p}}$ as the sum of the "noise-free" perfectly predicted measurements and an error term, $\mathbf{e}$,

$$\hat{\mathbf{p}} = \mathbf{G}\mathbf{f} + \mathbf{e}. \tag{22}$$

The optimal source strength vector $\mathbf{f}$ that minimises the sum of squared errors $\mathbf{e}^{\mathrm{H}}\mathbf{e}$, for the case where there are equal numbers of sources and sensors, is given by

$$\mathbf{f} = \mathbf{G}^{-1}\hat{\mathbf{p}}, \tag{23}$$

where H denotes the Hermitian transpose operator.

More generally, if there are more sensors than sources then the system of equations in Eq. (23) is over-determined. In this case $\mathbf{G}$ is non-square and the optimum solution is given by

$$\mathbf{f} = \mathbf{G}^{+}\hat{\mathbf{p}}, \tag{24}$$

where $\mathbf{G}^{+} = [\mathbf{G}^{\mathrm{H}}\mathbf{G}]^{-1}\mathbf{G}^{\mathrm{H}}$ is the pseudo-inverse of $\mathbf{G}$.

3.2. Application of the inversion technique to stationary broadband sources

Consider the cross-spectral matrix of measured pressures $\mathbf{S}_{\hat{\mathbf{p}}\hat{\mathbf{p}}}(\omega)$, defined by

$$\mathbf{S}_{\hat{\mathbf{p}}\hat{\mathbf{p}}} = E\left\{\frac{\pi}{T}\hat{\mathbf{p}}\hat{\mathbf{p}}^{\mathrm{H}}\right\}. \tag{25}$$

Substituting Eq. (21) into (25) gives

$$\mathbf{S}_{\hat{\mathbf{p}}\hat{\mathbf{p}}} = \mathbf{G}\mathbf{S}_{\mathbf{ff}}\mathbf{G}^{\mathrm{H}}, \tag{26}$$

where

$$\mathbf{S}_{\mathbf{ff}} = \lim_{T\to\infty} E\left\{\frac{1}{T}\mathbf{f}\mathbf{f}^{\mathrm{H}}\right\} \tag{27}$$

Similarly, to determine $\mathbf{S_{ff}}$ from $\mathbf{S_{\hat{p}\hat{p}}}$, Eq. (24) is substituted into Eq. (27) to give

$$\mathbf{S_{ff}} = \mathbf{G}^{+}\mathbf{S_{\hat{p}\hat{p}}}(\mathbf{G}^{+})^{\mathrm{H}}. \tag{28}$$

Note that the general expression for the pressure cross-spectrum given by Eq. (19) for rotating sources *cannot* be formulated in the form of Eq. (26) for stationary sources. The inversion procedure of Eq. (28) therefore does not apply to rotating sources. The essential difficulty, as made explicit by Eq. (19), is that the receiver and source frequencies are no longer the same. A procedure for determining the source strength in the rotating reference frame must therefore remove the effects of source rotation. Such a procedure is proposed below.

3.3. Inversion of rotating broadband sources

We begin with Eq. (17) for the pressure produced by a rotating single-frequency source distribution. Owing to the periodicity of the sound field in the θ direction, the pressure at the duct wall ($r = a$) at axial position z, sensed by N microphones at positions θ_n, can be written as a discrete Fourier series expansion with the coefficients

$$p_m(z, a, \omega) = \frac{1}{N}\sum_{n=1}^{N} p(a, \theta_n, z, \omega)\mathrm{e}^{-\mathrm{i}m\theta} \quad \left(\frac{-|1-N|}{2} \leqslant m \leqslant \frac{N}{2}\right). \tag{29}$$

This spinning mode decomposition gives the pressure amplitude, p_m, of the mth mode at the duct wall, and satisfies the Shannon sampling rate. Substituting Eq. (17) into Eq. (29) gives

$$p_m(z, a, \omega) = \int_{\tilde{S}} f(\tilde{\mathbf{y}}, \omega - m\Omega) g_m(\tilde{\mathbf{y}}, z, a, \omega)\, \mathrm{d}\tilde{S}(\tilde{\mathbf{y}}) \tag{30}$$

from which we may write,

$$p_m(z, a, \omega + m\Omega) = \int_{\tilde{S}} f(\tilde{\mathbf{y}}, \omega) g_m(\tilde{\mathbf{y}}, z, a, \omega + m\Omega)\, \mathrm{d}\tilde{S}(\tilde{\mathbf{y}}). \tag{31}$$

Eq. (31) suggests that the source spectrum at the unshifted frequency $f(\tilde{\mathbf{y}}, \omega)$ (i.e. observed in the rotating reference frame), can be deduced from measurements of the spinning mode amplitude $p_m(\mathbf{x}, \omega + m\Omega)$ and measurements (or predictions) of $g_m(\tilde{\mathbf{y}}, z, a, \omega + m\Omega)$ at a shifted frequency of $\omega + m\Omega$. The frequency shift is introduced to remove the effects of source rotation.

This frequency-shifted mode amplitude measurement p_m is now used to define a pressure spectrum $p_\Omega(\mathbf{x}, \omega)$, given by

$$p_\Omega(\mathbf{x}, \omega) = \sum_{m=-m^-}^{m^+} p_m(z, a, \omega + m\Omega)\mathrm{e}^{\mathrm{i}m\theta}, \tag{32}$$

where the subscript Ω on p is used to distinguish this pressure from the directly measurable pressure defined in Eq. (17). In Appendix A we show that the pressure p_Ω defined by Eq. (32) is precisely the same as that measured by a microphone rotating around the duct axis at the same angular speed as the rotor.

Note that the upper and lower limits of m in Eq. (32), $m^{\pm}$, specifying the range of propagating modes, differ from those in Eq. (17), $\pm m_0$ which contribute to the pressure measured by a stationary microphone in the duct. In Eq. (32), as m increases, so the frequency, $\omega + m\Omega$, at which the modal components p_m are evaluated also increases. Hence the summation over propagating modes has to be made over the new range of spinning mode orders, $-m^- \leqslant m \leqslant m^+$. The variation of m^+ and m^- with ka and Ω is examined in Section 3.4.

Substituting Eq. (31) into Eq. (32) leads to a relationship between the pressure p_Ω and the source strength $f(\tilde{\mathbf{y}})$, as observed in the rotating reference frame, $\tilde{\mathbf{y}}$,

$$p_\Omega(\mathbf{x}, \omega) = \int_{\tilde{S}} f(\tilde{\mathbf{y}}, \omega) \sum_{m=-m^-}^{m^+} g_m(\tilde{\mathbf{y}}, z, r, \omega + m\Omega)\mathrm{e}^{\mathrm{i}m\theta}\, \mathrm{d}\tilde{S}(\tilde{\mathbf{y}}). \tag{33}$$

By exact analogy with the expression for stationary source distributions, Eq. (33) for rotating sources can be formulated more generally as

$$p_\Omega(\mathbf{x},\omega)=\int_{\tilde{S}} f(\tilde{\mathbf{y}},\omega)\hat{\mathbf{n}}(\tilde{\mathbf{y}})\cdot\nabla G_\Omega(\tilde{\mathbf{y}},\mathbf{x},\omega)\,\mathrm{d}\tilde{S}(\tilde{\mathbf{y}}), \tag{34}$$

where G_Ω is a hard-walled duct Green function, which has been modified to incorporate the effects of source rotation, given by

$$G_\Omega(\tilde{\mathbf{y}},\mathbf{x},\omega)=\frac{\mathrm{i}}{4\pi}\sum_{m=-m^-}^{m^+}\sum_{n=0}^{n_0}\frac{\psi_{mn}(r)\psi^*_{mn}(r_s)\mathrm{e}^{\mathrm{i}m(\theta-\tilde{\theta}_s)}}{\Lambda_{mn}}\,\frac{\mathrm{e}^{-\mathrm{i}\gamma^{\pm}_{mn}(z-z_s)}}{\kappa_{mn}(\omega+m\Omega)} \tag{35}$$

and $\gamma^{\pm}_{mn}$ is evaluated at the shifted frequency $\omega+m\Omega$. Note that putting $\Omega=0$ in Eqs. (34) and (35) recovers Eq. (1) (expressed in the frequency domain) for the pressure due to stationary sources.

Eqs. (34) and (35) are therefore a generalised formulation of Eq. (1) for the acoustic pressure at a single frequency, which allows for the effects of source rotation. It is identical in form to that for stationary sources, and is suitable for inversion using existing techniques.

The analogous expression to Eq. (28) for the cross-spectrum of discretised rotating sources in the rotating reference frame in terms of the new Green function, $\mathbf{G}_\Omega$, is given by

$$\mathbf{S_{ff}}=\mathbf{G}^+_\Omega\mathbf{S}_{p_\Omega p_\Omega}(\mathbf{G}^+_\Omega)^{\mathrm{H}}. \tag{36}$$

Eq. (36) suggests that by use of this new Green function, G_Ω, the inversion procedure required to recover the source cross-spectrum $\mathbf{S}_{ff}(\tilde{\mathbf{y}},\tilde{\mathbf{y}}',\omega)$ in the rotating reference frame from measurements of the pressure cross-spectrum $\mathbf{S}_{p_\Omega p_\Omega}(\mathbf{x},\mathbf{x}',\omega)$ can be carried out in precisely the same way as for stationary broadband sources (Section 3.2). The important difference is that now the pressure cross-spectrum is computed from p_Ω, which first requires a spinning mode decomposition of the sound field to be performed.

Eqs. (35) and (36) form the main results of this paper. Their effectiveness for deducing the source strength of rotating source distributions is explored in Section 3.5. We first consider the determination of m^+ and m^-, corresponding to the range of propagating spinning modes contributing to P_Ω and $\mathbf{G}_\Omega$.

3.4. Determination of m^+ and m^-

The upper and lower modal orders m^+ and m^- appearing in Eq. (35) specify the range of propagating spinning modes that have to be included in the calculation of p_Ω and $\mathbf{G}_\Omega$ for sensors outside the near field of the rotor. With reference to Eq. (31), at least one radial mode of order m can propagate at a frequency $\omega+m\Omega$ providing $|\omega+m\Omega|>\omega_{m,0}$, where $\omega_{m,0}$ is the cutoff frequency of the lowest order radial mode $n=0$. This cut-off condition may be written in non-dimensional form as

$$|ka\pm mM_t|\geqslant(ka)_{m,0}, \tag{37}$$

where $(ka)_{m,0}=\sigma_{m,0}\sqrt{1-M^2}$ from Eq. (6), $M_t=\Omega a/c$ is the blade tip Mach number and ka is the non-dimensional observer frequency. Fig. 3 is a plot of the left-hand side of Eq. (37) (solid line) at $ka=20$ for a range of blade tip Mach numbers between 0 and 1.2. Also shown, indicated by circles, is the cuton frequency $(ka)_{m,0}$, corresponding to the right-hand side of Eq. (37). As indicated in Eq. (37) the mode m contains at least one propagating radial mode and must be included in the modal summation for m-values when the solid line is above the circles.

Fig. 3 shows that for supersonic tip speeds, $M_t>1$, the cutoff condition of Eq. (37) is satisfied for all m-values, $m>0$, since the two curves diverge for positive m. This suggests that all co-rotating spinning ($m>0$) modes to infinity must be included in the modal summation of p_Ω and G_Ω in Eq. (35). However only a finite number of counter-rotating modes ($m<0$) must be included. At the sonic blade tip speed $M_t=1$, the cuton frequency and "excitation frequency", $ka+mM_t$, increase with m at exactly the same rate and the curves run exactly parallel. Again all co-rotating mode orders to infinity must be included in p_Ω and G_Ω. For subsonic tip speeds, $M_t<1$, the two lines intersect indicating that there is always a finite range of co- and counter-rotating propagating mode orders that have to be included in the modal summation. Note that for $m<0$, irrespective of

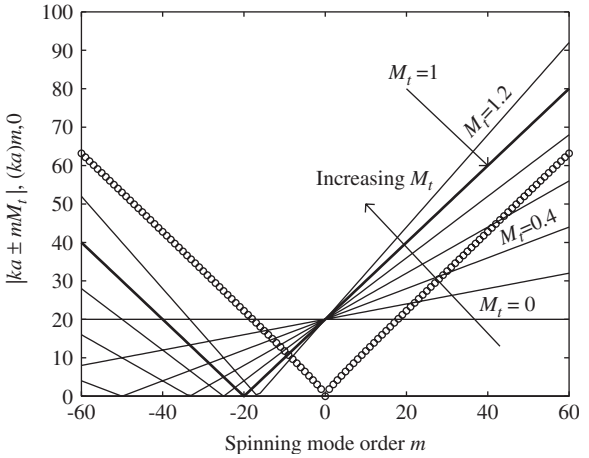

Fig. 3. A plot of azimuthal mode cuton frequencies $(ka)_{m,0}$ (○) and the left-hand side of the cuton condition $ka + mM_t$ (——) (Eq. (37)) versus mode order m for M_t values of 0 to 1.2 at normalised frequency $ka = 20$. Points of intersection define $m^{\pm}$.

M_t, the two curves always intersect, suggesting that there is always a finite range of counter-rotating modes to be included in p_Ω and G_Ω.

A good estimate for $m^{\pm}$ is obtained by noting that for suitably high m-values, in the absence of axial flow, the angular phase velocity c_p of the mode m at the duct wall is given by $c_p = a\omega/m$, which must exceed the speed of sound c_0 in order to propagate. Recalling that p_Ω is identical to the pressure measured by a microphone rotating around the duct wall at the shaft rotational frequency Ω. In this rotating reference frame, the cut-off condition becomes $c_p - a\Omega > c_0$. Substituting the approximation to c_p given above, this condition may be written as[1]

$$\frac{ka}{m} - M_t \geqslant 1. \tag{38}$$

Solving for $m = m^{\pm}$ in Eq. (37) gives

$$m^{\pm} = \frac{ka}{1 \mp M_t}. \tag{39}$$

Eq. (39) confirms that $m^{+} \to \infty$ as $M_t \to 1$, as predicted by Fig. 3.

3.5. Source resolution limits of the inversion technique for sensor arrays outside the near field of the rotor

We now quantify the resolution limits of the inversion technique, i.e how closely two sources may be discriminated. We assume that the microphone arrays used are positioned at a distance far enough away from the source plane that the effect of evanescent modes on the measured pressure is negligible. The application of the inversion technique for rotating sources, given by Eq. (36), relies on being able to accurately invert the matrix $\mathbf{G}_\Omega$. Error bounds on the source strength deduced from the inversion in the presence of measurement error, modelling error and other sources of noise, can be estimated from the *condition number* of $\mathbf{G}_\Omega$.

Consider the error $\delta\mathbf{f}$ in $\mathbf{f}$ due to errors (noise) $\delta\mathbf{p}_\Omega$ in the measured pressure $\mathbf{p}_\Omega$ under the transformation of Eq. (23),

$$\mathbf{f} + \delta\mathbf{f} = \mathbf{G}_\Omega^{+}(\mathbf{p}_\Omega + \delta\mathbf{p}_\Omega). \tag{40}$$

It can be shown [10] that the ratio of the norms of the perturbed quantities satisfies the inequality,

$$\frac{\|\delta\mathbf{f}\|}{\|\mathbf{f}\|} \leqslant \kappa(\mathbf{G}_\Omega)\frac{\|\delta\mathbf{p}_\Omega\|}{\|\mathbf{p}_\Omega\|}, \tag{41}$$

[1]Note that this cutoff condition can also be derived from Eq. (37) by noting that for large m-values, $(ka)_{m,0} \approx m$.

where $\|\cdot\|$ denotes the matrix 2-norm and the condition number of $\mathbf{G}_\Omega$ can be calculated from

$$\kappa(\mathbf{G}_\Omega) = \|\mathbf{G}_\Omega\|\|\mathbf{G}_\Omega^+\|. \tag{42}$$

Eq. (41) states that the error in the reconstructed source strength vector $\mathbf{f}$ is bounded by $\kappa(\mathbf{G})$ times the relative error in the measured pressures $\mathbf{p}_\Omega$. A similar analysis shows that the error in $\mathbf{f}$ due to modelling error in the transfer matrix $\mathbf{G}_\Omega$ is bounded by

$$\frac{\|\delta\mathbf{f}\|}{\|\mathbf{f}\|} \leqslant \kappa(\mathbf{G}_\Omega)\frac{\|\delta\mathbf{G}_\Omega\|}{\|\mathbf{G}_\Omega\|}. \tag{43}$$

In the following sections we investigate the effect on the conditioning of the matrix $\mathbf{G}_\Omega$ due to various assumed source distributions. These will be used to establish fundamental limits for how closely together the discrete rotating sources can be resolved. All the simulations will be performed without the addition of noise, $\delta\mathbf{p}_\Omega = 0$. Very large condition numbers ($\kappa(\mathbf{G}_\Omega) > 10^6$) will indicate that the results obtained by the inversion are likely to be very inaccurate when deduced from pressure measurements contaminated by small levels of noise.

The matrix $\mathbf{G}_\Omega$ relates the pressure $\mathbf{p}_\Omega$ measured at an array of microphones to the discretised source distribution $\mathbf{f}$. The choice of microphone positions will therefore affect the conditioning of $\mathbf{G}_\Omega$. Previous work by Kim and Nelson [5] has investigated the effect of microphone array geometry on $\kappa(\mathbf{G})$ for the case of stationary sources. Since the technique presented in this paper allows rotating sources to be inverted in precisely the same way as for stationary sources, these findings are also relevant to this work.

Kim and Nelson have examined the effect on $\kappa(\mathbf{G})$ of various wall-mounted microphone array configurations. They showed that there must be more microphones than sources in order for the transfer matrix to be well conditioned. It was found that the arrangement of the sensors into single, or multiple, axially separated rings did not have a significant influence on the condition number. Recall that, in the present technique, the measurement of p_Ω requires a modal decomposition to be preformed. In the following simulations, therefore, the microphone array consists of a single ring of N sensors sufficient in number to perform a modal decomposition at the highest frequency of interest, $N = 2m^+ + 1$, where m^+ is the highest "spatial frequency" of interest when cutoff modes can be neglected.

3.5.1. Angular resolution limits

We first examine, by means of a numerical simulation, the variation of $\kappa(\mathbf{G}_\Omega)$ as a function of the angular source separation angle $\Delta\theta$. In practical terms, this is a measure of the ability of the inversion technique to resolve sources on adjacent blades. In this simulation, N_s sources located at $r_s = 0.8a$ are arranged with an angular separation of $\Delta\theta = 2\pi/N_s$. The duct contains an axial mean flow of $M = 0.2$. The simulation is performed at a frequency of $ka = 15$ for various M_t-values. Eq. (39) suggests that $m^+ = \frac{15}{1-0.6} \approx 40$ at the highest M_t value under consideration here, $M_t = 0.6$, which therefore requires 80 sensors in a single ring to perform its modal decomposition. A single ring of 80 microphones is positioned 1 m downstream of the sources. At this measurement location and frequency, cutoff modes can be neglected.

The results of this simulation of $\kappa(\mathbf{G}_\Omega)$ versus $\Delta\theta$ as Fig. 4 (obtained by varying N_s) at different rotational speeds, M_t. As the number of sources N_s increases, an angular separation is reached where the condition number of $\mathbf{G}_\Omega$ suddenly becomes very large ($\kappa(\mathbf{G}_\Omega) > 10^{15}$) and therefore the sources can no longer be resolved.

By inspection, it is found that the angular resolution limit, $\Delta\theta$, below which the inversion is impractical due to poor conditioning of the transfer matrix, is given by

$$\Delta\theta \leqslant \frac{2\pi}{m_T}, \tag{44}$$

where $m_T = m^+ + m^- + 1$ is the total number of propagating azimuthal modes included in the calculation of $\mathbf{G}_\Omega$ for a given ka and rotational frequency Ω. This limit, $2\pi/m_T$, is indicated by the vertical dotted lines in Fig. 4. For $\mathbf{G}_\Omega$ to be well-conditioned there must be more azimuthal modes included in its calculation than there are sources. As shown in Fig. 3, and quantified by Eq. (39), m^+ increases with M_t and hence the angular resolution limit of the inversion technique improves as the tip speed Mach number increases.

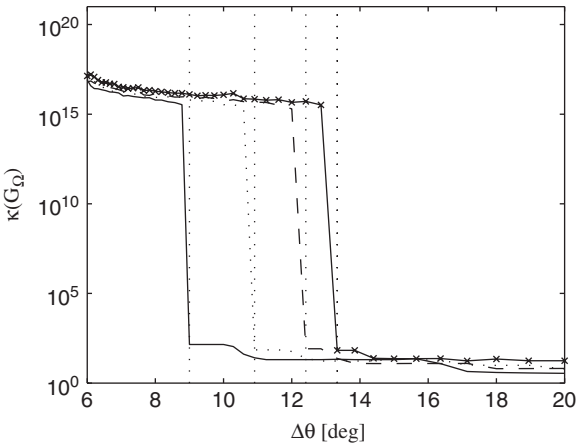

Fig. 4. Conditioning of the transfer matrix $\mathbf{G}_\Omega$ at $ka = 15$, as a function of azimuthal source separation for varying source rotational speeds (—×—, $M_t = 0$; - - -, $M_t = 0.3$; ....., $M_t = 0.45$; ——, $M_t = 0.6$). The vertical dotted lines indicate the value $2\pi/m_T$ calculated for each rotational speed.

3.5.2. Frequency limits for resolving sources on B blades

The angular resolution limits presented in the previous section have practical implications for the inversion of blade-based sources in aeroengines. If a blade can be represented by dipole source distribution along the trailing edge (or leading edge in the case of rotor/stator interaction noise where $\Omega = 0$) then in order to invert for the sources on B blades, an angular resolution of $2\pi/B$ must be possible. Putting $\Delta\theta = 2\pi/B$ and $m_T = m^+ + m^- + 1$ in Eq. (44), and noting Eq. (39) for m^+ and m^-, gives the following necessary, but not sufficient condition, for accurate inversion

$$\frac{ka}{1 - M_t} + \frac{ka}{1 + M_t} + 1 \gtrapprox B. \tag{45}$$

Eq. (45) establishes a lower frequency limit below which the sources on B blades cannot be resolved. Solving for this frequency and normalising by the blade passing frequency, $(ka)_{\mathrm{BPF}} = M_t B$, gives

$$\frac{\omega}{\omega_{\mathrm{BPF}}} = \frac{ka}{(ka)_{\mathrm{BPF}}} \gtrapprox \frac{(B-1)(1 - M_t^2)}{2M_t B}. \tag{46}$$

For large values of B typical of turbofan engines, Eq. (46) simplifies further to

$$\frac{\omega}{\omega_{\mathrm{BPF}}} \gtrapprox \frac{1 - M_t^2}{2M_t}. \tag{47}$$

Eq. (47) predicts that in order to resolve sources above a frequency $\alpha \cdot \omega_{\mathrm{BPF}}$ the blade tip Mach number must exceed $M_t = \sqrt{\alpha^2 + 1} - \alpha$. Source resolution above $\frac{1}{2}$ BPF and 1 BPF for example, is only possible at rotational speeds above $M_t = \sqrt{5/4} - 1/2 \approx 0.62$ and $\sqrt{2} - 1 \approx 0.41$, respectively. This lower limit falls rapidly as M_t is increased. To demonstrate this, $\omega/\omega_{\mathrm{BPF}}$ in Eq. (47) is plotted versus M_t in Fig. 5.

3.5.3. Radial resolution limits

Kim and Nelson [4] have shown that a half-wavelength resolution limits exists for inversion techniques when measurements are made in the far-field of the source. Assuming that the same resolution limit can also be applied to sources in a duct resolution limit for resolving sources radially in a duct can be shown to be,

$$\frac{n_{\max}}{N_s} > 1. \tag{48}$$

Since $n_{\max}$ may be interpreted, approximately, as the number of turning points of the mode shape function of the axi-symmetric mode $m = 0$. Correspondingly, it specifies, approximately, the number of half-wavelengths across the duct radius.

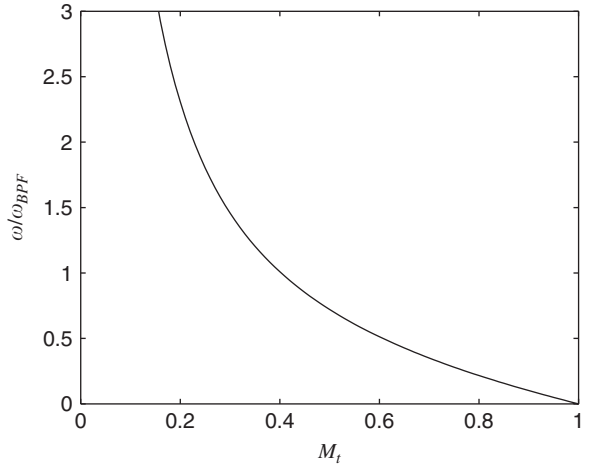

Fig. 5. The lower frequency limit, $\omega/\omega_{\mathrm{BPF}}$ for resolving sources azimuthally as a function of tip speed Mach number.

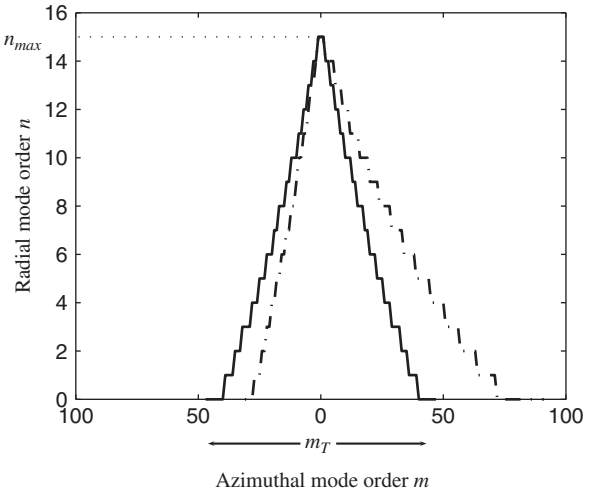

Fig. 6. The mode triangle at $ka = 50$ for stationary (——, $M_t = 0$) and rotating (– - –, $M_t = 0.5$) sources. The x-axis denotes the propagating azimuthal mode order m, the y-axis the highest order propagating radial mode associated with each of the azimuthal modes.

The dependence of resolution limits due to source rotation can be summarised by considering the "mode triangle", plotted in Fig. 6 for $M_t = 0$ and 0.5 at $ka = 50$ in which the number of radial modes is plotted against each spinning mode order included in the calculation of $\mathbf{G}_\Omega$. The result for the stationary source case, $M_t = 0$, is a symmetrical triangle. For $M_t = 0.5$, the triangle is skewed towards the co-rotating modes ($m^+ > m^-$ as explained in Section 3.4). As predicted by Eq. (44) azimuthal resolution therefore improves as source rotational speed increases. Note that in Fig. 6 the highest radial order mode $n_{\max}$ in both the stationary and rotating source cases is associated with the $m = 0$ azimuthal mode, irrespective of Ω. The maximum radial order therefore does not increase with increasing source rotation frequency. The inequality in Eq. (48) is therefore valid for all rotational speeds, and the radial resolution limit is only weakly dependent on Ω.

Section 3.5.2 has shown that attempting to invert for sources on different blades leads to a lower frequency limit below which the inversion cannot be performed. We now propose a simplifying assumption that not only substantially reduces the number of sources to be inverted but also circumvents the resolution problem identified in Section 3.5.2.

4. Simplifying assumption for the blade surface pressure cross-spectrum

A general expression for the sound field produced by rotating sources in a duct has been derived in Eq. (19). For the case of an aeroengine fan some further simplifying assumptions can be made in order to reduce considerably the number of sources to be inverted.

We first assume that the acoustic sources are concentrated along the trailing edge of each individual rotor blade and that the sources on different blades are uncorrelated. The source spatial cross-spectrum of Eq. (20) may therefore be written as

$$S_{ff}(\tilde{\mathbf{y}},\tilde{\mathbf{y}}',\omega)=S_{ff}(r_s,r_s',\tilde{\theta}_{s_0},\omega)\delta(\theta_{s_p}-\theta_{s_p}')\delta(\theta_{s_p}-2\pi p/B)\quad(z_s=z_s'),\tag{49}$$

where δ is the Dirac delta function, B is the number of blades and $\theta_{s_p}=2\pi p/B$ specifies the angular position of the pth trailing edge (where $p=0,\ldots,B-1$).

Noting that $\mathrm{d}\tilde{S}(\tilde{\mathbf{y}})=r_s\,\mathrm{d}r_s\,\mathrm{d}\tilde{\theta}$, and assuming that the pressure measurements are made at the duct wall $r=a$, Eq. (33), for $S_{p_\Omega p_\Omega}$ for B *identical*, uncorrelated blades reduces to,

$$\begin{aligned}S_{p_\Omega p_\Omega}(\mathbf{x},\mathbf{x}',\omega)=B\int_{r_s}\int_{r_s'}\sum_{m=-m_0}^{m_0}\sum_{m'=-m_0}^{m_0}&S_{ff}(r_s,r_s',\tilde{\theta}_{s_0},\omega)\\&\times g_m(r_s,\tilde{\theta}_{s_0},z,a,\omega+m\Omega)g_m^*(r_s',\tilde{\theta}_{s_0},z',a,\omega+m'\Omega)\mathrm{e}^{\mathrm{i}m\theta-\mathrm{i}m'\theta'}r_sr_s'\,\mathrm{d}r_s\,\mathrm{d}r_s',\end{aligned}\tag{50}$$

where $\tilde{\theta}_{s_0}$ is the circumferential position of the zeroth blade, $p=0$ (chosen arbitrarily).

We now investigate the accuracy of the inversion procedure by applying it to "measurements" of $\mathbf{S}_{p_\Omega p_\Omega}$ predicted using a model for S_{ff} in Eq. (50). The rotor blade is modelled as a smooth, flat plate with zero pressure gradient. For simplicity scattering of the hydrodynamic pressure field by the trailing edge is ignored in the model for S_{ff} and the surface pressure fluctuations are assumed to be concentrated at the blade trailing edge. We use the simple model given by Blake [11] to represent the spatial correlation function, S_{ff}, of the pressure fluctuations beneath a turbulent boundary layer on a flat plate, which has the form

$$S_{ff}(r_s,r_s',\omega)=\Phi_{ff}(r_s,\omega)\mathrm{e}^{-\gamma\frac{\omega|r_s-r_s'|}{U_c}},\tag{51}$$

where Φ_{ff} is the frequency pressure spectrum of the turbulence boundary layer, and γ is an empirical constant determined from experiment. Further details of the model are given in Appendix B. Eq. (51) may be used to define the boundary layer correlation length, L_c, as the spanwise separation distance $|r_s-r_s'|$ at which S_{ff} attains half its maximum value,

$$L_c=\frac{\ln(0.5)U_c}{-\gamma\omega}.\tag{52}$$

For practical purposes, the source model of Eq. (51) must be discretised for numerical evaluation of Eq. (50). The number of sources, and hence their separation distance along the blade span, required in the calculation of S_{ff} from Eq. (51) is determined by examining the convergence of $S_{p_\Omega p_\Omega}$ predicted as a function of the number of uncorrelated sources.

Fig. 7 is a plot of the magnitude and phase of the cross-spectrum $S_{p_\Omega p_\Omega}$ as a function of source separation distance for various rotational speeds M_t. The "measured" pressure cross-spectrum is observed to converge as the source separation distance tends to a turbulence correlation length L_c. In order to obtain a converged model for S_{ff} in Eq. (50) therefore, discrete sources used to model the boundary layer pressure distribution of Eq. (51), must be separated by at least one correlation length at the frequency of interest.

Recall from Section 3.5.3 that for measurements made outside the near field of the rotor, sources can only be resolved with a separation distance greater than approximately $\lambda/2$. The correlation length, L_c, may be compared with this resolution limit by noting that $U_c\approx 0.7\sqrt{(\Omega r)^2+(Mc)^2}$ and $\gamma=0.7$ in Eq. (52) to give

$$\frac{L_c}{\frac{1}{2}\lambda}\approx\frac{M_t}{10}.\tag{53}$$

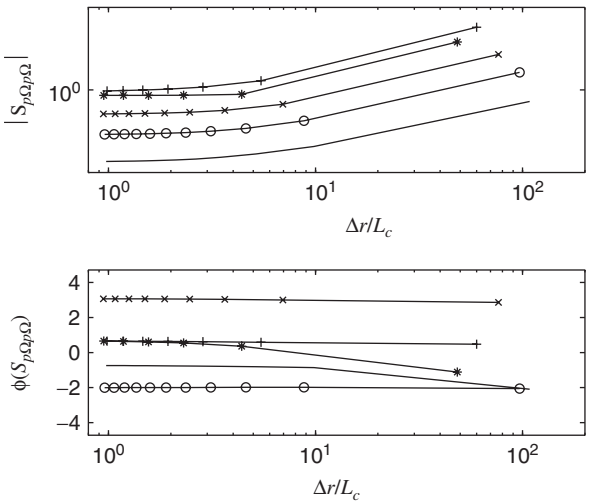

Fig. 7. Convergence of the magnitude (top) and phase (bottom) of $S_{p_\Omega p_\Omega}$ as a function of source separation distance as measured by a pair of microphones situated at the duct wall with an angular separation of 10°. Convergence at varying source rotational speeds is plotted : ($M_t = 0$ (——), $M_t = 0.2$ (—○—), $M_t = 0.4$ (—×—), $M_t = 0.6$ (—+—), $M_t = 0.8$ (—×—)).

The source separation distance required to give a converged value of S_{ff} is therefore significantly less, by an order of magnitude, than the separation distance, $\lambda/2$, that can be resolved using measurements made outside of the near field of the rotor. Eq. (53) implies that for these measurements the inversion must assume fewer sources, by at least a factor of ten, than the effective number of uncorrelated sources present on the rotor blades. The performance of the inversion technique for this situation will now be investigated.

4.1. Application of the inverse technique to the "single-blade" model

Eq. (50) gives the pressure cross-spectra at a particular microphone position due to a fan with B identical blades. The discretised version of this equation, following the procedure presented in Section 3.1, is

$$\mathbf{S}_{p_\Omega p_\Omega} = B\mathbf{G}_\Omega \mathbf{S}_{\mathbf{ff}} \mathbf{G}_\Omega^{\mathrm{H}}. \tag{54}$$

The determination of $\mathbf{S}_{\hat{f}\hat{f}}$ from measurements of $\mathbf{S}_{p_\Omega p_\Omega}$ follows from Eq. (54) as

$$\mathbf{S}_{\hat{f}\hat{f}} = \frac{1}{B}\mathbf{G}_\Omega^{+}\mathbf{S}_{p_\Omega p_\Omega}\mathbf{G}_\Omega^{+\mathrm{H}}. \tag{55}$$

A schematic diagram of the source geometry used in this simulation is shown in Fig. 8. The uncorrelated sources, representing the aerodynamic trailing edge noise in the forward problem, are shown as small circles separated by a turbulence correlation length L_c. The assumed sources, used in the inverse problem, with a separation distance Δr, are denoted by the larger circles.

The accuracy of the inversion is computed from the normalised error function defined by

$$J_{ff} = \frac{\|\mathbf{S}_{ff} - \mathbf{S}_{\hat{f}\hat{f}}\|}{\|\mathbf{S}_{ff}\|}, \tag{56}$$

where $\mathbf{S}_{ff}$ is the source strength cross-spectrum of the exact aerodynamic sources at the location of the assumed sources.

In order to improve upon the resolution limits identified in Section 3.5 obtained for measurements made away from the rotor near field requires measurements to be made in the acoustic near field. For this region the sound field comprises high wavenumber components. This necessitates the inclusion of cutoff modes in the calculation of $\mathbf{G}_\Omega$ and in the measurement of p_Ω.

The inversion is performed at $ka = 15$ and $M_t = 0.5$ for various axial measurement positions between $|z - z_s| = 0.05\lambda$ and $|z - z_s| = 10\lambda$. The turbulence correlation length of the aeroacoustic sources, from

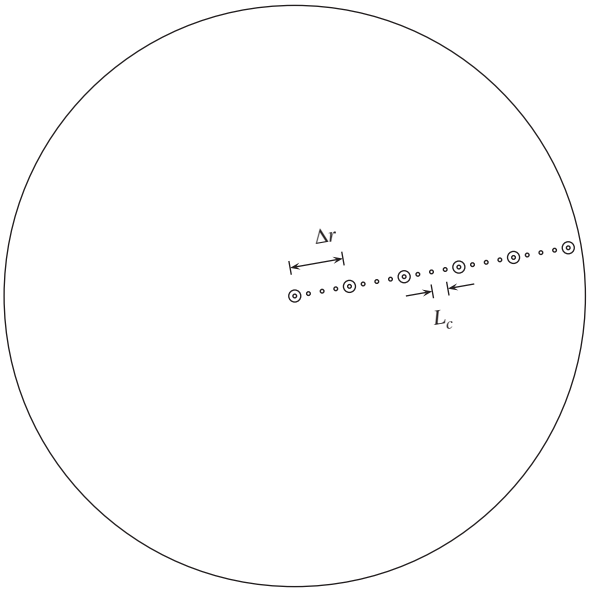

Fig. 8. A schematic of the geometry of the inversion technique for aerodynamic sources. The uncorrelated sources, representing the aerodynamic trailing edge noise in the forward problem, are shown as small circles separated by a turbulence correlation length L_c. The assumed sources, used in the inverse problem, with a separation distance Δr are denoted by larger circles.

Eq. (52) is 0.0148 m. For a duct with a 1 m radius, therefore, $a/L_c \approx 68$ sources are used in the forward problem to calculate the cross-spectra $S_{p_\Omega p_\Omega}$ at the measurement positions. Note that the number of cutoff modes included in the calculation is chosen to give a converged solution of p_Ω and $\mathbf{G}_\Omega$.

The pressure measurements used in this inversion could be obtained in practice by a radial "rake" with the same number of sensors as assumed sources, equally spaced along a single radius from the centre of the duct to the duct wall. The pressure cross-spectrum $\mathbf{S}_{p_\Omega p_\Omega}$ is calculated at the microphone positions using Eq. (54). The inversion is performed using Eq. (55) with varying numbers of assumed sources equally spaced along a radius (as illustrated in Fig. 8). Fig. 9 is a plot of the inversion accuracy J_{ff} (Eq. (56)) and the conditioning of the transfer matrix $\kappa(\mathbf{G}_\Omega)$, as a function of the separation distance, Δr, between assumed sources for varying source–microphone axial separation distances, $|z - z_s|$.

Fig. 9 indicates that good inversion accuracy and acceptable conditioning values are only possible simultaneously for microphones positioned closer than approximately $\lambda/3$ from the source plane. Fig. 10 shows some illustrative results for the inverted source strength magnitudes along the blade trailing edge (crosses, the diagonal elements of the $\mathbf{S}_{\hat{f}\hat{f}}$ matrix). Also shown are the exact source strengths used in the converged model for $\mathbf{S}_{ff}$ (circles).

Fig. 10 shows that, with approximately one assumed source per two correlation lengths (Fig. 10a), with microphones positioned 0.05λ from the source plane, it is possible to achieve a reconstruction of the source strength distribution that agrees well with the exact source strength distribution. However, $\kappa(\mathbf{G}_\Omega)$ is very high ($>10^6$) in this example. Errors in the reconstructed source strengths are most apparent at the tip of the blade, $r_s = a$. Figs. 10b and d suggest that moving the microphone array further from the rotor requires fewer sources to be assumed in order to ensure good conditioning. However, the reconstruction accuracy deteriorates as a result. Assuming the same number of sources at $|z - z_s| = 0.1\lambda$ as at $|z - z_s| = 0.05\lambda$ (Fig. 10c) results in poor conditioning, and hence poor agreement, between reconstructed and exact source strengths.

In order to improve the reconstruction accuracy further, it would be necessary to move the microphones even closer to the source plane. This might be difficult to achieve in practice, and would require an even greater number of sensors to perform the modal decomposition for the determination of p_Ω. Steps would also have to be taken to minimise contamination of the measurements by flow noise. At $ka = 15$ and $|z - z_s| = 0.1\lambda$, the

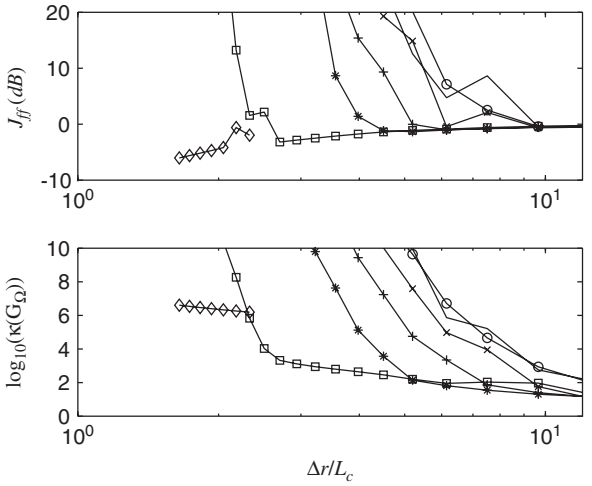

Fig. 9. A plot of the inversion accuracy J_{ff} and the conditioning of the transfer matrix $\kappa(\mathbf{G}_\Omega)$ as a function of the distance between assumed sources ($\Delta r/L_c$). The simulation is carried out for various source–microphone separation distances ($|z-z_s|/\lambda = 10$ (——), $|z-z_s|/\lambda = 1$ (—○—), $|z-z_s|/\lambda = 0.5$ (—×—), $|z-z_s|/\lambda = 0.3$ (—+—), $|z-z_s|/\lambda = 0.2$ (—×—), $|z-z_s|/\lambda = 0.1$ (—□—), $|z-z_s|/\lambda = 0.05$ (—◇—)). Measurement in the near-field allows more sources to be assumed, and therefore improves the reconstruction accuracy, at the expense of conditioning.

maximum azimuthal mode order, m^+, included in the calculation of $\mathbf{G}_\Omega$ is 100. Practical application of the inversion technique at this frequency would therefore require the determination of the amplitudes of all modes up to this order.

Positioning the microphones close to the rotor would in practice increase the significance of cascade effects (multiple reflections of the sound radiated from the trailing-edges between adjacent blades). In principle, these effects could be taken into account in the formulation of the measured or predicted Green functions. An indication of the significance of cascade effects on trailing edge noise is provided by the work of Glegg [12] who has shown that, to a good approximation, radiation from the cascade is related to that from an isolated airfoil by a simple frequency dependent multiplicative factor, that varies between 0 and 2.

The results in this paper suggest that there is a balance to be struck between the reconstruction accuracy, J_{ff}, and the conditioning $\kappa(\mathbf{G}_\Omega)$. Based on the data presented in this paper, a suitable compromise is to make measurements 0.1λ from the source plane, assuming approximately one source for every 3 turbulence correlation lengths. This allows source strengths to be estimated to around 1 dB accuracy, with a conditioning that is low enough for robust inversion ($\kappa(\mathbf{G}_\Omega) \approx 2000$) to be performed. Conditioning could be improved further by the application of matrix regularisation techniques, such as those investigated in the context of in-duct inversion problems by Kim and Nelson [5]. However this is usually achieved at the expense of reduced inversion accuracy.

5. Conclusion

An inversion technique suitable for the determination of rotating, broadband sources in a duct has been presented. This work is an extension of the work of Kim and Nelson [5] for the inversion of stationary ducted monopoles and the work by Sijtsma et al. [1] of a rotating beamformer for the measurement of sources on an open rotor.

The principle findings presented in this paper may be summarised as follows:

- The rotation of sources in a duct causes a coupling between source and propagation terms. Existing inversion techniques therefore cannot be used for the determination of aerodynamic sources on rotor blades.

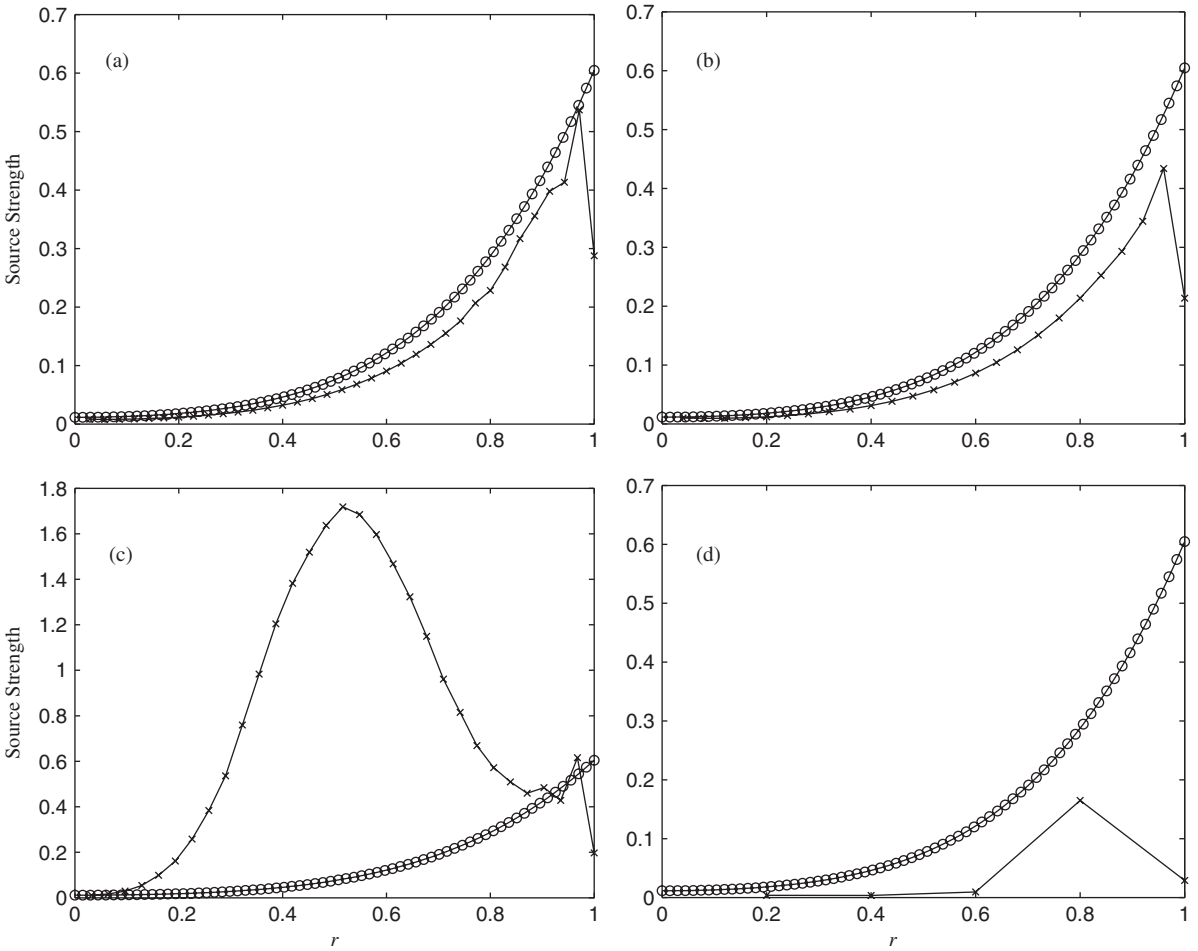

Fig. 10. Reconstruction of radial source strengths at $ka = 15$ with near-field effects. Plotted are the true source strengths (—○—) and the reconstructed source strengths (—×—) as a function of radial distance. The source–receiver separation distance, conditioning of the transfer matrix and radial spacing between assumed sources in each case are as follows (a) $|z - z_s| = 0.05\lambda$, $\kappa(\mathbf{G}_\Omega) = 2.48 \times 10^6$, $\Delta r/L_c = 1.93$. (b) $|z - z_s| = 0.1\lambda$, $\kappa(\mathbf{G}_\Omega) = 2068$, $\Delta r/L_c = 2.70$. (c) $|z - z_s| = 0.1\lambda$, $\kappa(\mathbf{G}_\Omega) = 1.85 \times 10^8$, $\Delta r/L_c = 2.18$. (d) $|z - z_s| = 0.1\lambda$, $\kappa(\mathbf{G}_\Omega) = 12.8$, $\Delta r/L_c = 13.5$.

- A measurement technique has been developed to deduce the pressure spectrum that is precisely equal to that measured by microphones rotating around the duct axis at the same rotational speed as the fan.
- Based on this new measurement technique, and the introduction of a new Green function, which includes the effects of source rotation, a new inversion technique has been devised that allows the determination of the strength of rotating, broadband sources in their rotating reference frame.
- The resolution limits of the new inversion technique, for measurements made outside the near field of the rotor, have been shown to be significantly larger than the effective separation distance of uncorrelated sources located on the fan blade trailing edge. To improve upon the resolution limits therefore, measurements must be made in the near field of the rotor, requiring the use of a much larger number of sensors to decompose the azimuthal modes.
- Simulations have demonstrated that for a 26-bladed fan, rotating at $M_t = 0.5$, the aerodynamic source strengths can be estimated with acceptable robustness and approximately 1 dB accuracy, when measurements are made 0.1 acoustic wavelengths from the rotor.

Appendix A. Interpretation of p_Ω

In this appendix it is shown that the pressure p_Ω is the pressure that would be measured by a microphone rotating around the duct axis at the same angular frequency Ω as the source distribution.

If the microphones are made to rotate around the duct axis at an angular frequency Ω, so that $\theta = \tilde{\theta} - \Omega t$, where $\tilde{\theta}$ is the angular position of the sensor in the rotating reference frame, Eq. (15) for the time varying acoustic pressure measured by the rotating microphones becomes

$$p(\tilde{\mathbf{x}}, t) = \int_{\tilde{S}} \sum_{m=-m^-}^{m^+} f(\tilde{\mathbf{y}}, \omega - m\Omega) \int_{-\infty}^{\infty} \sum_{n=0}^{n_0} \left[\gamma_{mn}^{\pm} \cos\beta + \frac{m}{r_s} \sin\beta \right] \times \frac{\psi_{mn}(r)\psi_{mn}^*(r_s) e^{im(\tilde{\theta}-\tilde{\theta}_s)}}{\Lambda_{mn}} \int_{-\infty}^{\infty} \frac{e^{i(\omega - m\Omega)t} e^{-i\gamma_{mn}^{\pm}(z-z_s)}}{\kappa_{mn}(\omega)} \, d\omega \, d\tilde{S}(\tilde{\mathbf{y}}), \tag{A.1}$$

where $\tilde{\mathbf{x}}$ is the measurement position in the rotating reference frame $\tilde{\mathbf{x}} = [r, \tilde{\theta}, z]$.

Fourier transforming Eq. (A.1) with respect to t,

$$p(\tilde{\mathbf{x}}, \omega') = \frac{1}{2\pi} \int_{-\infty}^{\infty} p(\tilde{\mathbf{x}}, t) e^{-i\omega' t} \, dt \tag{A.2}$$

gives the frequency spectrum as observed by the rotating microphone as

$$p(\tilde{\mathbf{x}}, \omega') = \int_{\tilde{S}} \int_{-\infty}^{\infty} \sum_{m=-m^-}^{m^+} f(\tilde{\mathbf{y}}, \omega - m\Omega) g_m(\tilde{\mathbf{y}}, r, x, \omega) \delta(\omega - \omega' - m\Omega) e^{im\tilde{\theta}} \, d\omega \, d\tilde{S}(\tilde{\mathbf{y}}) \tag{A.3}$$

i.e.,

$$p(\tilde{\mathbf{x}}, \omega') = \int_{\tilde{S}} \sum_{m=-m^-}^{m^+} f(\tilde{\mathbf{y}}, \omega') g_m(\tilde{\mathbf{y}}, r, x, \omega' + m\Omega) e^{im\tilde{\theta}} \, d\tilde{S}(\tilde{\mathbf{y}}). \tag{A.4}$$

Comparison of Eq. (A.4) with Eq. (33) shows that

$$p(\tilde{\mathbf{x}}, \omega) = p_\Omega(\mathbf{x}, \omega). \tag{A.5}$$

The two equations are therefore identical with $\mathbf{x} = \tilde{\mathbf{x}}$. This suggests that the acoustic pressure, p_Ω defined by Eq. (34) is precisely equivalent to that measured by the sensors rotating at the shaft rotational velocity Ω in which the sources appear stationary.

Appendix B. Flat plate turbulence model

In the flat-plate turbulence model used in Section 4 γ is an experimentally determined constant, typically 0.7 and the turbulent eddy convection velocity, U_c, over a flat plate, is approximately related to the free stream velocity U_∞ by

$$U_c = 0.7 U_\infty. \tag{B.1}$$

The single-point frequency spectrum of wall pressure fluctuations $\Phi_{ff}(r_s, \omega)$ in Eq. (51) is [11]

$$\Phi_{ff}(\omega, r_s) \propto \begin{cases} \rho_0^2 U_\tau^4 (\delta/U_c)(\omega\delta/U_c)^2 & \text{for } \dfrac{\omega\delta}{U_c} \leqslant 1, \\ \rho_0^2 U_\tau^4 \omega^{-1} & \text{for } 1 < \dfrac{\omega\delta}{U_c} \leqslant \dfrac{\frac{1}{30} U_\tau \delta}{\nu}, \\ \rho_0^2 (U_\tau^4)^{-1} (\omega\delta/U_c)^{-4} & \text{for } \dfrac{\omega\delta}{U_c} > \dfrac{\frac{1}{30} U_\tau \delta}{\nu}, \end{cases} \tag{B.2}$$

where U_τ, δ and U_c all vary with radial position r_s along the blade. The turbulent boundary layer thickness is approximately [11]

$$\delta = \frac{c}{Re_c^{0.2}}, \tag{B.3}$$

where c is the rotor chord length, v is the kinematic viscosity and Re_c the Reynolds number cU_∞/v defined with respect to c.

In Eq. (B.2) the hydrodynamic friction velocity U_τ, is an experimentally defined ratio which for a smooth flat plate [11] is $U_\tau/U_\infty = 0.037$.

References

[1] P. Sijtsma, S. Oerlemans, H. Holthusen, Location of rotating sources by phased array measurements, *Seventh AIAA/CEAS Aeroacoustics Conference*, Maastricht, Netherlands 2001.
[2] J. Billingsley, R. Kinns, The acoustic telescope, *Journal of Sound and Vibration* 48 (4) (1976) 485–510.
[3] M.J. Fisher, K.R. Holland, Measuring the relative strengths of a set of partially coherent acoustic sources, *Journal of Sound and Vibration* 201 (1) (1997) 103–125.
[4] Y. Kim, P. Nelson, Spatial resolution limits for the reconstruction of acoustic source strength by inverse methods, *Journal of Sound and Vibration* 265 (3) (2003) 583–608.
[5] Y. Kim, P.A. Nelson, Estimation of acoustic source strength within a cylindrical duct by inverse methods, *Journal of Sound and Vibration* 275 (1–2) (2004) 391–413.
[6] E. Williams, *Fourier Acoustics, Sound Radiation and Nearfield Acoustic Holography*, Academic Press, New York, 1999.
[7] K. Holland, P. Nelson, Sound source characterisation: the focused beamformer vs. the inverse method, *Proceedings of the Tenth International Congress on Sound and Vibration*, July 7–10 2003, Institute of Acoustics, Stockholm, Sweden, 2003, pp. 3499–3506.
[8] M.E. Goldstein, *Aeroacoustics*, McGraw-Hill, New York, 1976.
[9] C. Morfey, Sound transmission and generation in ducts with flow, *Journal of Sound and Vibration* 14 (1) (1971) 37–55.
[10] G. van Loan, *Matrix Computations*, North Oxford Academic, Oxford, 1983.
[11] W. Blake, *Mechanics of Flow Induced Sound and Vibration*, Vol. II, Academic Press, New York, 1986.
[12] S. Glegg, Airfoil self-noise generated in a cascade, *AIAA Journal* 36 (9) (1998) 1575–1582.